IOP Conf. Series: Materials Science and Engineering **375** (2018) 012034 doi:10.1088/1757-899X/375/1/012034

Texture, microstructure and mechanical properties evolution in Fe-x (x = 36 and 48 wt.%) Ni alloy after accumulative roll bonding

S Boudekhani-Abbas[1], K Tirsatine[1], H Azzeddine[1,2,*], B Alili[1], A L Helbert[3], F Brisset[3], T Baudin[3] and D Bradai[1]

[1] Faculty of Physics, University of Sciences and Technology Houari Boumediene, BP 32 El-Alia, 16111, Algiers, Algeria.
[2] Departments of Physics, University Mohamed Boudiaf, BP 166, 28000, M'Sila Algeria
[3] ICMMO, SP2M, Univ. Paris-Sud, Université Paris-Saclay, UMR CNRS 8182, 91405 Orsay Cedex, France
*Corresponding author: azehibou@yahoo.fr

Abstract. The texture, microstructure and Vickers microhardness evolution of Fe-36Ni and Fe-48Ni (wt. %) alloys processed by accumulative roll-bonding (ARB) up to 6 cycles were investigated using Electron Back Scatter Diffraction (EBSD) and microhardness measurements. Both alloys underwent a substantial grain refinement. Grains were of elongated shape parallel to the rolling direction and slightly smaller for Fe-48Ni alloy. Both alloys exhibit a different texture evolution upon straining influenced by the deformation conditions. The microhardness of both alloys also showed the same trends up to 6 cycles and Fe-48Ni alloy has higher strength than Fe-36Ni alloy. These differences were mainly ascribed to the deformation conditions, solute pinning and stacking fault energy.

1. Introduction

Severe plastic deformation (SPD) techniques such as equal channel angular pressing (ECAP) [1], high-pressure torsion (HPT) [2] and accumulative roll bonding (ARB) [3] have proven their ability to produce Ultra-Fine Grain (UFG) materials with high strengthening [4]. Up to now, among SPD techniques, only ARB processing has a great potential to be adapted to the industry in order to produce UFG materials in the form of large sheets due to its possibility as continuous process [5]. The evolution of crystallographic texture strongly depends on the SPD techniques [5–8]. Moreover, SPD techniques can lead to significant changes in the texture evolution compared to the conventional ones such as compression or rolling. Texture that develops after ARB processing is generally characterized by rolling-type components at the mid-thickness and shear-type components near the surface [5, 6]. However, there is a strong lack of studies on the effect of some special parameters such as deformation temperature, sample preparation or solute content on microstructure, texture and mechanical properties.

The aim of the present work is to investigate the effect of solute content on the texture, microstructure and mechanical properties evolution after severe plastic deformation of a Fe-x (x=36 and 48 wt.%) Ni alloy by ARB processing.

2. Experimental Procedure

The Fe-36%Ni (wt.%) and Fe-48%Ni (wt.%) alloys sheets were kindly provided by APERAM alloy society in France. ARB processing was carried out on a two-high mill of 2.2 kW power with rolls of 67 mm in diameter and rotating speed was 14 s^{-1}. Between cycles the Fe-36Ni and Fe-48Ni samples were preheated at 550 °C and 350°C for 10 min, respectively. The ARB processing was repeated up to 6 cycles.

Microstructure and microtexture were characterized using a scanning electron microscope FEG-SEM SUPRA 55 VP operating at 20 kV with OIM^{TM} software. For EBSD measurements, the Fe-36Ni and Fe-48Ni samples were cut in the cross-section (RD-ND plan, rolling direction-normal direction) near the mid-thickness and to the surface of samples, respectively and were mechanically polished and then electropolished. The quantitative texture analysis was carried out by calculating the Orientation Distribution Function (ODF) using MTex software [9].

The Vickers microhardness of the samples was measured by SHIMADZU type HMV-2 tester using a load of 0.05 kg ($HV_{0.05}$) and indentation time of 10 seconds.

3. Results and discussion

Figure 1 presents the inverse pole figure (IPF) maps in the (RD-ND) plane showing the microstructure of the Fe-36Ni and Fe-48Ni alloys after ARB processing up 6 cycles. The EBSD maps reveal a substantial grain refinement and the grains are elongated parallel to the rolling direction. Figure 2 demonstrates the evolution of High angle grain boundaries (HAGB), the length (L along rolling direction) and the thickness (l along normal direction) of Fe-36Ni and Fe-48Ni ultrafine grains. The HAGB fraction decreases after 1 cycle leading to the formation of low angle grain boundaries (LAGB) due to the subdivision of primary grains and formation of subgrains.

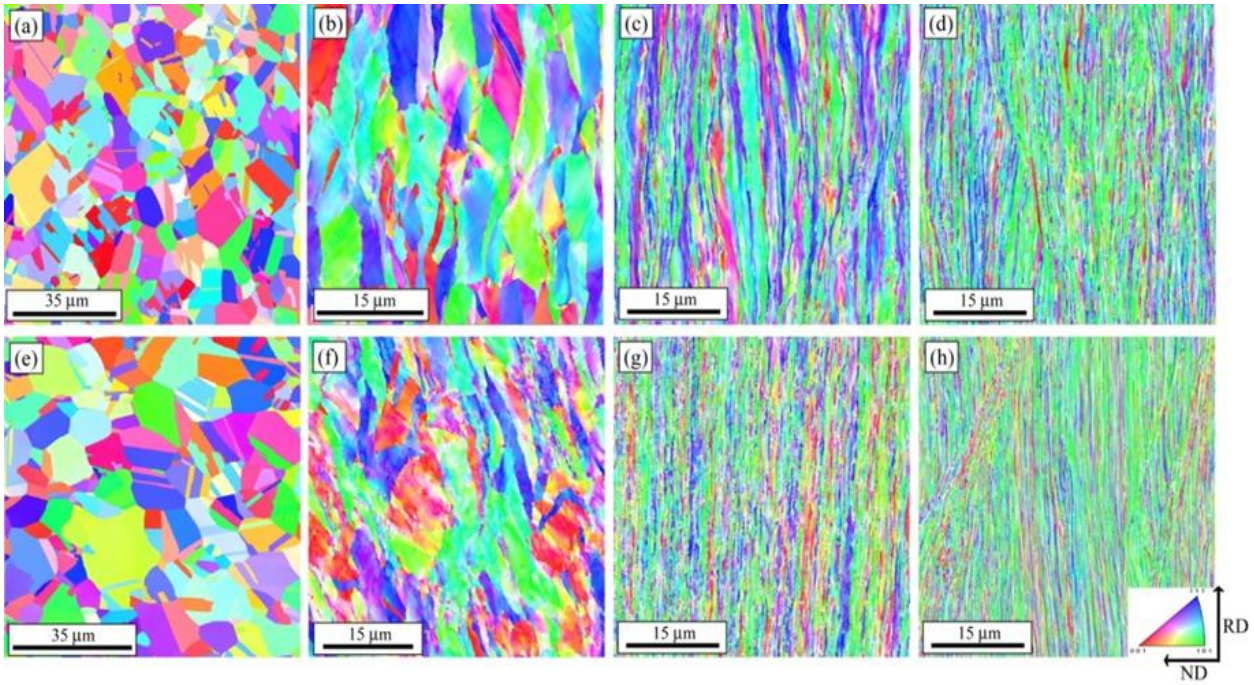

Figure 1: IPF maps showing the microstructure evolution of Fe-36Ni: a) 0 cycle, b) 1 cycle, c) 3 cycles, d) 6 cycles and of Fe-48Ni: e) 0 cycle, f) 1 cycle, g) 3 cycles and h) 6 cycles.

Then, the HAGB increases with increasing number of ARB cycles because of dislocation accumulation and the transformation of subgrain boundaries to HAGB to saturate near 68 % after 4 cycles for Fe-36Ni and 74 % after 5 cycles for Fe-48Ni. For both alloys the grain size parameters (L

and l) decrease with increasing number of ARB cycles and saturate after 4 cycles. It is interesting to note that Fe-48Ni alloy produces slightly smaller grain size compared to Fe-36Ni alloy due the effect of solute pinning on grain boundary migration [10].

The effect of heating treatment between cycles could also affect the final grain size by promoting dynamic recovery of dislocation [11]. In fact, during ARB processing the Fe-36Ni sample was heated at 550 °C for 10 min which is a suitable temperature for recrystallization (~ 600 °C) [12]. Although, the Fe-48Ni sample was treated at 350 °C which is far less than the effective temperature for recrystallization resulting hence in smaller grain size.

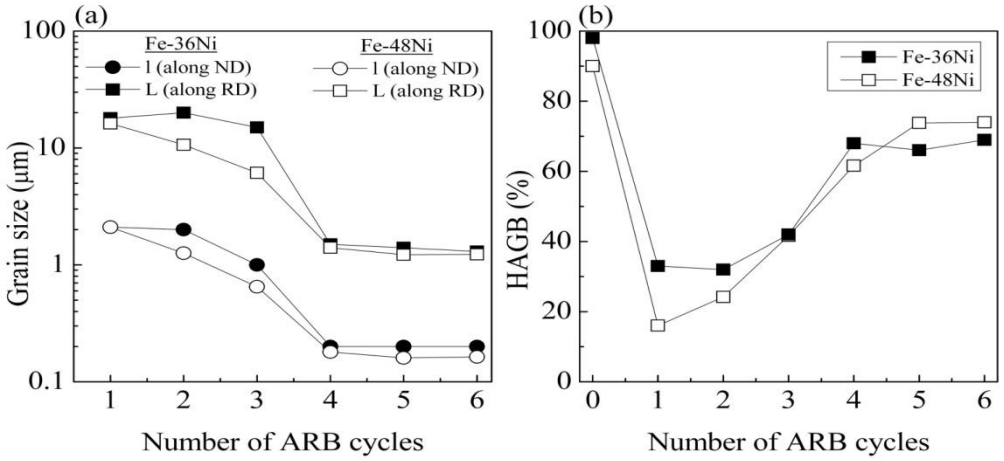

Figure 2: (a) Grain size parameters (length along RD (L) and ND (l)) and (b) HAGB fraction of Fe-36Ni and Fe-48Ni alloys as function of number of ARB cycles.

Figure 3 presents the texture evolution of Fe-36Ni and Fe-48Ni alloys upon straining via ODF sections (φ_2 = 0, 45 and 65°). The main ideal texture component position of FCC alloys is also presented and their descriptions are given in Table 1. The EBSD measurements were carried out in the cross section near to the mid-thickness of the Fe-36Ni sample where no shear components have been detected [5]. By contrast, the EBSD data of the Fe-48Ni samples were collected in the cross section near to the surface of the samples, where the shear texture is dominated by the R-Cube component [5].

Table 1: Main ideal rolling texture components of FCC alloys.

Component	**{hkl}<uvw>**	**Euler Angle**		
		φ_1	Φ	φ_2
□ Brass	{110}<112>	35°	35°	45°
◇ Goss	{110}<001>	0°	45°	0°
● Cube	{001}<100>	0°	0°	0°
○ R-Cube	{001}<110>	45°	0°	0°
△ Copper	{112}<111>	90°	35°	45°
▽ S	{231}<346>	59°	29°	63°

Obviously, Fe-36Ni and Fe-48 alloys exhibit a different texture evolution. The Fe-36Ni alloy, with a strong Cube initial texture, developed a Brass component (after 1 cycle) and finally a Copper-type texture (Brass, S and Copper components) after 6 cycles. The Fe-48Ni alloy, with a quasi-random initial texture, developed a Rotated-Cube component after 1 cycle with is a typical shear texture component and subsequently a Copper component dominated after 6 cycles. This is in good agreement

with results of Jamaati et al. [13] who assumed that the shear (R-Cube) components present in the surface regions of the sample could rapidly rotate towards rolling components as soon as they are moved to the quarter thickness regions. Indeed, a simulation with VPSC has confirmed this assumption [6]. It is interesting to note that Brass component has not been developed in Fe-48Ni alloy during ARB processing. Instead of Brass component a new weak (1.9 mrd) component {012}<2$\bar{2}$1> (43°, 24°,0°) has been development (ODF section at φ_2 =0°) starting from 3 cycles. Such texture component was already reported in Fe-36Ni alloy after cross ARB [6].

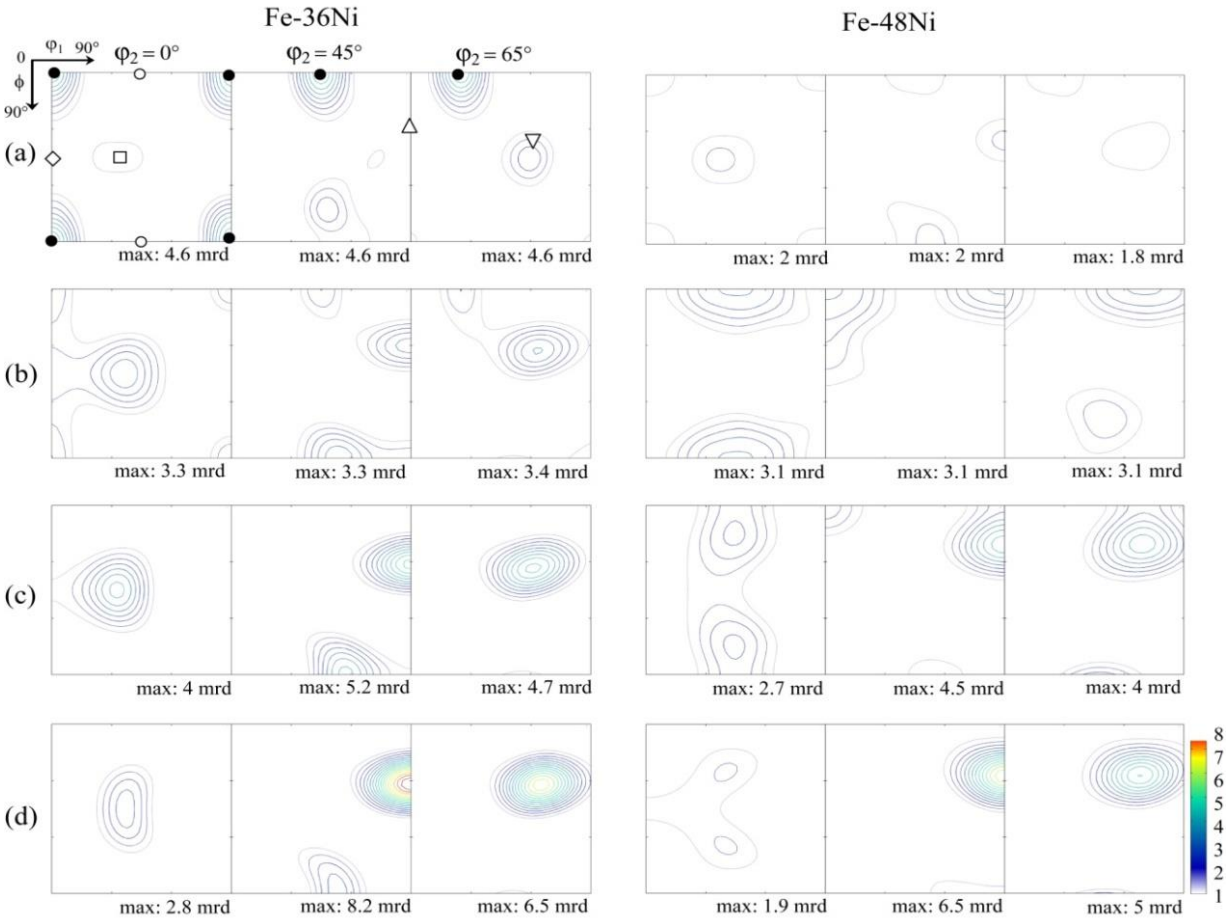

Figure 3: ODF sections at φ_2 =0, 45 and 65° of Fe-36Ni and Fe-48Ni alloys after ARB processing: a) 0 cycle, b) 1 cycle, c) 3 cycles and d) 6 cycles.

The evolution of microhardness of Fe-36Ni and Fe-48Ni alloys after nnnARB processing is shown in Figure 4. For both alloys, Hv increased up 3 cycles due to the combination of dislocation generation and grain refinement [14]. After 3 cycles the Hv values tends to stabilize well probably due to the occurrence of a concurrent dynamic recovery process [15]. It is interesting to note that the Hv values of Fe-48Ni alloy are almost 10 % higher that Fe-36Ni ones. This difference can be attributed to the effect of deformation temperature. It is known that the micorhardness decrease with increasing deformation temperature [16] mainly to due to the grain refinement Moreover, the difference in Hv values should probably arise from the stacking fault energy variation between the two alloys. An estimation of the reduced stacking fault energy γ_{SFE}/Gb has been done using an empirical correlation

between it and the ratio of Brass (V_{Brass}), Copper (V_{Copper}) and S (V_S) volume fractions as proposed in the literature [17]:

$$\frac{\gamma_{SFE}}{Gb} \propto \frac{2V_{Brass}}{V_{Copper}+V_S} \quad (1)$$

where G is the shear modulus and b the Burgers vector.

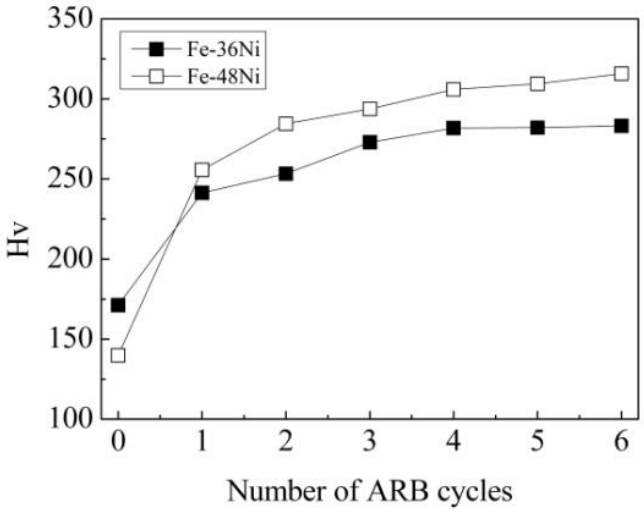

Figure 4: Microhardness evolution of Fe-36Ni and Fe-48Ni alloy as function of number of ARB cycles.

Table 2 listed the estimated γ_{SFE} for Fe-36Ni and Fe-48Ni alloy after ARB processing. The deduced values are surprisingly in good agreement with the literature data [18]. Indeed, the Fe-48Ni exhibits a lower γ_{SFE} compared to Fe-36Ni alloy. Many authors have demonstrated that a reduction in SFE leads to a smaller grain size and increased strength and ductility in FCC deformed alloys [19, 20]. Following these authors, the higher strength was mainly due to grain refinement and higher density of twins formed during deformation processing. In fact, as the SFE decreased, the stacking faults became wider, making cross-slip more difficult. Hence, mechanical twinning was favored. It is well known that low stacking fault energy promotes strain hardening due to the inhibition of dynamic recovery process by suppression of cross slipping and this leads to the fast build-up of the critical dislocation density required for initiating twinning [21].

Table 2. Estimation of the Stacking Fault Energy γ_{SFE}.

γ_{SFE} (mJ/m^2)	1 cycle	3 cycles	6 cycles	Reference
Fe-36Ni	124.7	127.6	128.6	122 [17]
Fe-48Ni	74.2	75.4	81.2	78 [17]

For both alloys, the γ_{SFE} values seem to increase with increasing strain but this increase is not significant and lies within the relative error estimated to be ± 8 mJ/m^2. In the author's opinion, no systematic evolution of the stacking energy versus amount of straining should exist but only versus solute content.

4. Conclusion

- The Fe-36Ni and Fe-48 Ni (wt. %) alloys after ARB processing at 550 and 350 °C up to 6 cycles respectively, underwent a substantial grain refinement. Grains are of elongated shape parallel to the rolling direction and slightly smaller for Fe-48Ni alloy.
- Both alloys exhibit a different texture evolution upon straining. The Fe-48Ni alloy developed a Rotated-cube component after 1 cycle and subsequently a domination of Copper component after 6 cycles. While, the Fe-36Ni alloy developed a Brass component after 3 cycles and finally a Copper-type texture after 6 cycles.
- The microhardness of both alloys showed the same trends up to 6 cycles. That of Fe-48Ni alloy was higher than that of Fe-36Ni owing to its smaller stacking fault energy.

Acknowledgements
This work was supported in part by the PHC Maghreb Program N°16MAG03.

References

[1] Valiev R Z, Islamgaliev R K and Alexandrov I V 2000 *Prog. Mater. Sci.* **45** 103–189.
[2] Smirnova N A, Levit V I, Pilyugin V I, Kuznetsov R I, Davidova L S and Sazonova V A 1986 *Phys. Met. Metall.* **61** 127-134.
[3] Saito Y, Tsuji N, Utsunomiya H, Sakai T and Hong R G 1998 *Scripta Mat.* **39** 1221-27.
[4] Valiev R Z, Estrin Y, Horita Z, Langdon T G, Zehetbauer M and Zhu Y T 2006 *JOM* **58** 33–39.
[5] Tirsatine K, Azzeddine H, Baudin T, Helbert A L, Alili B and Bradai D 2014 *J. Alloys Compd.* **610** 352-360.
[6] Azzeddine H, Tirsatine K, Baudin T, Helbert A L, Brisset F and Bradai D 2014 *Mater. Charact.* **97**140–149.
[7] Khereddine Y, Hadj Larbi F, Azzeddine H, Baudin T, Brisset F, Helbert A L, Mathon M, Kawasaki M, Bradai D and Langdon T G 2013 *J. Alloys Compd.* **574** 361–367.
[8] Hadj Larbi F, Azzeddine H, Baudin T, Mathon M H, Brisset F, Helbert A L, Kawasaki M, Bradai D and Langdon T G 2015 J. Alloys Compd. 638 88–94.
[9] Bachmann F, Hielscher R and Schaeben H 2010 *Solid. State. Phenom.* **160** 63–68.
[10] Hersent E, Marthinsen K and Nes E 2013 *Metall and Mat Trans* A **44** 3364–75.
[11] Pirgazi H, Akbarzadeh A, Petrov R, Sidor J and Kestens K 2008 *Mat. Sci. Eng.* A **492** 110-117.
[12] Zaefferer S, Baudin T and Penelle R 2001 *Acta Mater.* **49** 1105–22.
[13] Jamaati R and Toroghinejad M R 2014 *Mat. Sci. Eng.* A. **598** 263–276.
[14] Hansen N, Huang X and Hughes D A 2001 *Mat Sci Eng.* A **317** 3–11.
[15] Kumar S S S and Raghu T 2011 *Materials and Design* **32** 4650–57.
[16] Mungole T, Nadammal N, Dawra K, Kumar P, Kawasaki M and Langdon T G 2013 *J Mater Sci* **48** 4671–80.
[17] Witte M, "Texture Optimization of Ni-5at.%W for Coated Conductor Application", Diss. RWTH Aachen University, 2013.
[18] Schramm R E and Reed R P 1976 *Metall. Trans.* A **7** 359–363.
[19] Pei-Ling S., Zhao Y H, Cooley J C, Kassner M E, Horita Z, Langdon T G, Lavernia E J and Zhu Y T 2009 *Mat. Sci. Eng.* A. **525** 83–86.
[20] Zhao Y H, Zhu Y T, Liao X Z, Horita Z and Langdon T G 2006 *Appl. Phys. Lett.* **89** 121906.
[21] El-Danaf E A, Soliman M S and Al-Mutlaq A A 2015 *Adv. Mater. Sci. Eng.* **2015** 1–12.